ACS APPLIED MATERIALS & INTERFACES

Research Article

www.acsami.org

Temozolomide Nanoparticles for Targeted Glioblastoma Therapy

Chen Fang,[†,‡] Kui Wang,[‡] Zachary R. Stephen,[‡] Qingxin Mu,[†,‡] Forrest M. Kievit,[§] Daniel T. Chiu,[∥] Oliver W. Press,[†,⊥] and Miqin Zhang*[,‡,§]

[†]Clinical Research Division, Fred Hutchinson Cancer Research Center, Seattle, Washington 98109, United States

[‡]Department of Materials Science and Engineering, University of Washington, Seattle, Washington 98195, United States

[§]Department of Neurological Surgery, University of Washington, Seattle, Washington 98195, United States

[∥]Department of Chemistry, University of Washington, Seattle, Washington 98195, United States

[⊥]Departments of Medicine and Bioengineering, University of Washington, Seattle, Washington 98195, United States

ABSTRACT: Glioblastoma (GBM) is a deadly and debilitating brain tumor with an abysmal prognosis. The standard therapy for GBM is surgery followed by radiation and chemotherapy with Temozolomide (TMZ). Treatment of GBMs remains a challenge, largely because of the fast degradation of TMZ, the inability to deliver an effective dose of TMZ to tumors, and a lack of target specificity that may cause systemic toxicity. Here, we present a simple method for synthesizing a nanoparticle-based carrier that can protect TMZ from rapid degradation in physiological solutions and can specifically deliver them to GBM cells through the mediation of a tumor-targeting peptide chlorotoxin (CTX). Our nanoparticle, namely NP-TMZ-CTX, had a hydrodynamic size of <100 nm, exhibited sustained stability in cell culture media for up to 2 weeks, and could accommodate stable drug loading. TMZ bound to nanoparticles showed a much higher stability at physiological pH, with a half-life 7-fold greater than that of free TMZ. NP-TMZ-CTX was able to target GBM cells and achieved 2−6-fold higher uptake and a 50−90% reduction of IC_{50} 72 h post-treatment as compared to nontargeted NP-TMZ. NP-TMZ-CTX showed great promise in its ability to deliver a large therapeutic dose of TMZ to GBM cells and could serve as a template for targeted delivery of other therapeutics.

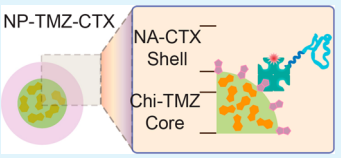

KEYWORDS: *glioblastoma, drug delivery, therapeutics, chlorotoxin, MGMT, nanomedicine*

INTRODUCTION

Glioblastoma (GBM) is a deadly and debilitating brain tumor with 14000 new cases diagnosed annually in the United States. Despite considerable efforts in patient care, the prognosis of GBM has remained dismal with a median survival of 12−14 months and a 5-year survival rate of less than 3%.[1,2] Standard treatment of GBM starts with surgery followed by concurrent radio- and chemotherapy. The widespread use of more effective, targeted treatments in the clinic has been hindered by (1) the heterogeneous cytogenetic nature of GBM that limits the use of pathway-specific targeted agents, (2) the diffuse infiltration of invasive GBM cells that precludes complete resection of cancerous tissue and thus recurrence after surgical resection is nearly inevitable, and (3) the presence of a blood−brain barrier (BBB) that renders the majority of chemotherapeutics and targeted agents ineffective.[2−5] Most recently, the anti-angiogenic antibody, bevacizumab (Avastin), which facilitated improved outcomes in recurrent GBM,[6] did not improve overall survival in newly diagnosed patients.[7] Therefore, there is an urgent need to develop novel therapeutic strategies to improve the survival and quality of life of GBM patients.

Temozolomide (TMZ) is the standard-of-care chemotherapy for GBM as first-line treatment with radiotherapy or as a single agent for maintenance therapy.[4] As a DNA-alkylating agent that methylates guanine and adenine bases of DNA, TMZ administered to GBM cells leads to DNA double-strand breaks, cell cycle arrest, and eventual cell death.[8] However, TMZ suffers from several drawbacks. TMZ attacks DNA in an indiscriminate manner and has been shown to cause damage to hematopoietic stem cells in patients,[9] resulting in dose-limiting hematological toxicity. Furthermore, TMZ is poorly soluble under physiological conditions and is subject to rapid hydrolysis that further limits its antitumor efficacy. Various strategies have been used to make TMZ target-specific by conjugating it to targeting moieties and to improve the aqueous stability of TMZ by incorporation into a macromolecular delivery vehicle.[10,11] However, these strategies did not address the necessity of glioblastoma-specific targeting or the problem of target antigen expression on normal cells.[10] These problems create a strong incentive to design a nanoparticle-based TMZ delivery system that is specific for glioblastoma and improves the solubility and stability of TMZ.

Previously, we demonstrated that nanoparticles (NPs) with chitosan-based coatings could be used for imaging and as effective delivery vehicles for transport of gene therapeutic agents to the brain.[12,13] Chitosan (Chi) is a cationic polysaccharide widely used in tissue engineering and drug/gene delivery applications. Chitosan contains abundant amine groups that can be utilized for covalent attachment of drugs, imaging agents, and targeting moieties. A number of targeting molecules have been evaluated to target GBM, including

Received: December 30, 2014
Accepted: March 9, 2015
Published: March 9, 2015

DOI: 10.1021/am5092165
ACS Appl. Mater. Interfaces 2015, 7, 6674−6682

chlorotoxin (CTX),[12−20] anti-epidermal growth factor receptor (EGFR) antibody,[21] and anti-transferrin receptor antibody.[10,22] Among these targeting ligands, CTX has several advantages. It has the ability to specifically recognize a variety of tumors of neuroectodermal origin, including GBM, while showing little affinity for normal brain.[18] After binding to GBM cells, NPs functionalized with CTX are readily internalized,[13] a favorable attribute for delivering drugs to their intracellular site of action. CTX has also been shown to inhibit GBM cell invasion, providing an additional therapeutic benefit.[19] Most importantly, the attachment of CTX to NPs coated with chitosan allows them to bypass the BBB,[12] and CTX provides an ideal platform for further development of chitosan-based systems as drug delivery vehicles for GBM.

Here, we present a targeted, chitosan-based NP TMZ delivery system (NP-TMZ-CTX) that can improve the stability of TMZ under physiological conditions and the efficacy of TMZ against GBM. NP-TMZ-CTX was assembled via biotin−neutravidin interaction without the need for additional purification. The size and stability of NP-TMZ-CTX were characterized using dynamic light scattering (DLS). The targeting ability and therapeutic efficacy for human GBM cells were assessed through flow cytometry and the CellTiter-Glo viability assay, respectively. Specific targeting was quantified with a microplate reader, and the intracellular distribution was visualized by deconvolution fluorescence microscopy. The ability of NP-TMZ-CTX to cross the BBB was demonstrated in vivo and examined via immunohistochemistry (IHC) and confocal fluorescence microscopy.

EXPERIMENTAL SECTION

Materials. All chemicals were purchased from Sigma-Aldrich (St. Louis, MO) unless otherwise noted. Chitosan oligosaccharide (MW of 3500) was purchased from Acmey Industrial Co. (Shanghai, China). PEG was grafted onto chitosan by reductive alkylation with methoxy-PEG-aldehyde (MW of 2000) following our previously established method.[23] Temozolomide (TMZ) was purchased from TCI America (Portland, OR). Temozolomide acid (TMZA) was synthesized from TMZ following a previously established method.[24] Biotin-PEG-valeric acid succinimidyl ester (Bt-PEG-SVA, MW of 5000) was purchased from Laysan Bio (Arab, AL). DMEM media, antibiotic-antimycotic (AA), fetal bovine serum (FBS), trysin/EDTA solution, Alexa Fluor 647 *N*-hydroxysuccinimidyl ester (AF647-NHS), wheat germ agglutinin Alexa Fluor 488 conjugates (WGA-AF488), Prolong Gold with DAPI (4′,6-diamidino-2-phenylindole dihydrochloride), and methanol-free formaldehyde (10%) were purchased from Life Technologies (Carlsbad, CA). The CellTiter-Glo Luminescent Cell Viability Assay Kit was purchased from Promega (Madison, WI). Poly-L-lysine-treated glass coverslips were purchased from Becton Dickinson (Franklin Lakes, NJ). Traut's reagent, SMPEG24, Zeba spin columns [40K molecular weight cutoff (MWCO)] were purchased from Thermo Fisher (Rockford, IL). Rabbit anti-mouse CD31 antibody and goat anti-rabbit Fc antibody-FITC conjugates were purchased from Abcam (Cambridge, MA). CTX (recombinant) was produced from *Escherichia coli* according to an established protocol.[25]

Synthesis of Chitosan-TMZ Conjugates. To synthesize chitosan-TMZ-Bt conjugates, the molar ratio of precursors was fixed at 1:7:40 (chitosan:Bt-PEG-VAS:TMZ). To make chitosan-biotin conjugates (Chi-Bt), 1000 mg of chitosan and 1867.2 mg of Bt-PEG-VAS were placed in a 20 mL vial. Triethylamine (219 μL) dissolved in 5 mL of DMSO was then added to the vial, and the vial was sealed and purged with nitrogen. The reaction was allowed to proceed in a shaker at room temperature for 24 h. The crude reaction product was precipitated from a DMSO solution using ether, vacuum-dried, and dissolved in 5 mL of 0.1 N HCl. This 0.1 N HCl solution was then dialyzed against deionized water overnight to remove any unreacted precursors. The solution was then lyophilized to obtain intermediate Chi-Bt in the form of a yellow solid. To synthesize Chi-TMZ-Bt, TMZA (50 mg) was first activated using thionyl chloride (500 μL) and DMF (31 μL).[24] Chi-Bt (200 mg) was dissolved in 4 mL of DMSO, and the resultant mixture was added to freshly prepared, activated TMZA in a 100 mL three-neck flask. Pyridine (219 μL) was added to the flask as a catalyst, and the reaction was allowed to proceed for 24 h to generate Chi-TMZ-Bt. The crude reaction product was precipitated from the DMSO solution using ether, vacuum-dried, and dissolved in 5 mL of 1 N HCl. The 1 N HCl solution of Chi-TMZ-Bt was dialyzed against 1 mM HCl for 6 h to remove unreacted precursors. The solution was then lyophilized to obtain the final product Chi-TMZ-Bt as a yellow solid.

Synthesis of NA-AF647-CTX and Formation of NPs. To synthesize NA-AF647-CTX conjugates, stock neutravidin (NA) solutions were prepared in deionized water at 25 mg/mL. The NA solution was then diluted in borate-buffered saline with EDTA [25 mM sodium tetraborate, 150 mM sodium chloride, and 5 mM EDTA (pH 8.3)], to achieve a final NA concentration of 10 mg/mL. AF647-NHS (100 μL at 10 mg/mL in DMSO) was added to a 900 μL NA solution, and the reaction was allowed to proceed for 3 h at room temperature. NA-AF647 was purified by Zeba spin columns (40K MWCO) equilibrated with 50 mM sodium phosphate (pH 7.4). At the same time, 1 mg of CTX in 100 μL of 50 mM sodium phosphate (pH 7.4) was reacted with 2.15 μL of Traut's reagent solution [10 mg/mL in 50 mM sodium phosphate (pH 7.4)] for 1 h. To synthesize NA-AF647-CTX, 1.96 μL of SMPEG24 (250 mM in DMSO) was added to 1 mg of a NA-AF647 solution, and the reaction was allowed to proceed in the dark for 30 min. The resulting NA-AF647-PEG_{24}Mal was purified by Zeba spin columns (40K MWCO) equilibrated with 0.9% saline.

The AF647 loading of NA-AF647-CTX was determined by UV−vis absorbance at 649 nm (AF647 absorbance maximum) and 280 nm (protein absorbance). The amount of CTX grafted onto NA was determined by sodium dodecyl sulfate−polyacrylamide gel electrophoresis of the NA-AF647-CTX reaction mixture. Subtracting the concentration of free CTX remaining in the solution from the concentration of CTX at the beginning of the reaction provided the amount of immobilized CTX.

To synthesize NP-TMZ-CTX, the Chi-TMZ-Bt solution was reconstituted in pH 4.0 saline and the pH of NA-CTX solution was adjusted to 4.0 with 1 N HCl. These two solutions were combined at a NA:Bt molar ratio of 1:1. The final product was obtained after a 30 min incubation. Synthesis of NP-TMZ-NA followed the same method as that of NP-TMZ-CTX.

Characterizations of NPs and Controlled Drug Release. The sizes and ζ potentials of NPs were measured by dynamic light scattering (DLS) using a DTS Zetasizer Nano (Malvern Instruments, Worcestershire, U.K.). NP concentrations were 100 μg/mL for all measurements. NP stability was determined in PBS and DMEM containing 2.5% FBS and 1% AA.

Transmission electron microscopy (TEM) imaging was conducted with an FEI Tecnai G2 F20 200 kV scanning transmission electron microscope (FEI Co., Hillsboro, OR). Images of NPs were captured by a liquid nitrogen-cooled charge-coupled device (CCD) camera. NP samples in water were deposited on a carbon-coated copper grid (Ted Pella Inc., Redding, CA) and negatively stained with uranyl acetate.

Drug loading was determined by measuring the absorbance of polymer or dissolved NP solutions using a UV−vis spectrometer (Agilent Technologies, Santa Clara, CA). The wavelength of UV absorption for TMZ was 328 nm.

For the measurement of drug release, 1 mL NP samples (equivalent TMZ concentration of 1 mg/mL) were dispersed in PBS buffer at pH 7.4, 6.4, 5.5, or 4.5 and incubated at 37 °C. Aliquots (100 μL) were removed from the bulk solution at 0.5, 1, 2, 3, 6, 9, 12, and 24 h. The absorbance was obtained using the UV−vis spectrometer at 328 nm for active TMZ {the degradation product of TMZ, MTIC [5-(3-methyltriazen-1-yl)imidazole-4-carboxamide], does not absorb at 328 nm} and corrected with the intrinsic absorbance of chitosan at 328

DOI: 10.1021/am5092165
ACS Appl. Mater. Interfaces 2015, 7, 6674−6682

Scheme 1. Schematic of NP-TMZ-CTX Synthesis[a]

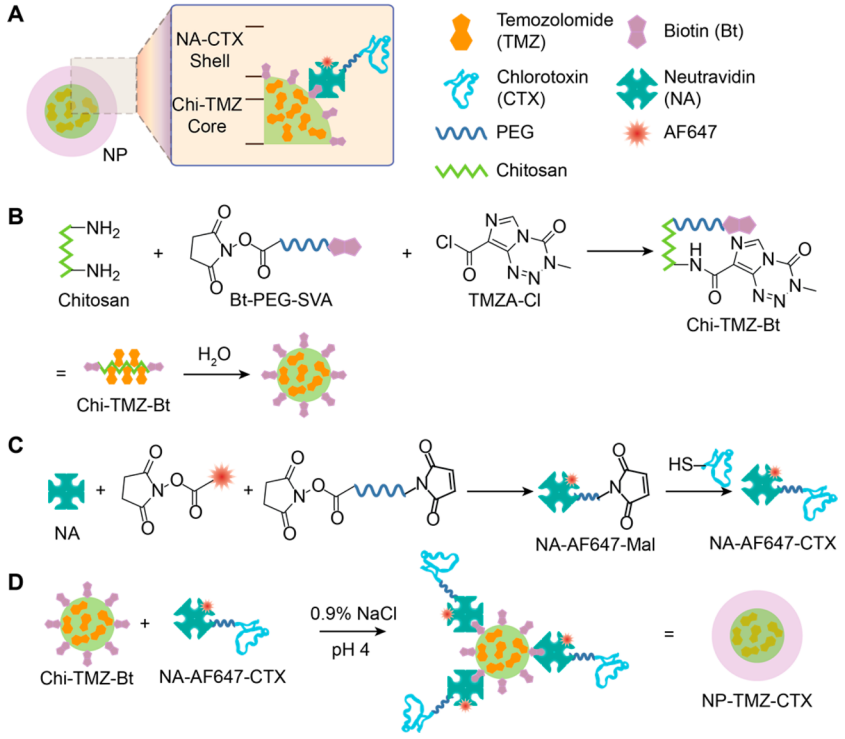

[a](A) Structure of NP-TMZ-CTX. (B) Synthesis of Chi-TMZ-Bt. (C) Synthesis of NA-AF647-CTX. (D) Formation of NP-TMZ-CTX by linking Chi-TMZ-Bt and NA-AF647-Bt via Bt-NA interactions.

nm. The percent release of TMZ ($R_{\%}$) was calculated using the following equation:

$$R_{\%} = [1 - (A_{\text{NP-TMZ}} - A_{\text{Chi}})/E_{\text{TMZ}}] \times 100\%$$

where $A_{\text{NP-TMZ}}$ is the absorbance of TMZ in bulk solution, A_{Chi} is the absorbance of chitosan copolymer without TMZ at the same concentration, and E_{TMZ} is the extinction coefficient of TMZ.

Dose–Response Experiment. Human GBM cell line U-118 MG was obtained from American Type Culture Collection (ATCC, Manassas, VA). SF767 and GBM6 were gifts from the Brain Tumor Research Laboratory, UCSF,[26] and the Sarkaria laboratory, Mayo Clinic,[27] respectively. GBM cells were maintained in DMEM containing 2.5% FBS and 1% AA at 37 °C in 95%/5% humidified air/CO_2 atmosphere.

All GBM cells were plated at a density of 5000 cells per well in 96-well plates immediately prior to treatment. Cells were then exposed to free TMZ, NP-TMZ, or NP-TMZ-CTX at 0, 20, 200, 2000, 20000, and 200000 ng/mL TMZ in 200 μL of fully supplemented DMEM. Cell viability was determined 72 h after initial exposure using the CellTiter-Glo viability assay following the manufacturer's protocol. IC_{50} values were calculated from dose–response curves generated with a polynomial dose–response four-parameter approximation using GraphPad Prism (GraphPad Software Inc., La Jolla, CA).

Cell Uptake Experiment and Fluorescence Imaging. For cell uptake quantification experiments, all cells were plated at a density of 100000 cells per well in 24-well plates the night before treatment. Cells were then treated with 5, 25, or 250 μM NP-TMZ-NA or NP-TMZ-CTX in 1 mL of fully supplemented DMEM for 12 h. Cells were washed three times with PBS and then solubilized with 500 μL of 2.4 M HCl. The fluorescence intensity of AF647 was measured with a SpectraMax M5 microplate reader (Molecular Devices, Union City, CA), using excitation and emission wavelengths of 647 and 670 nm, respectively. The cell number per well was assessed using a Coomassie Blue protein quantification assay and calculated on the basis of a previously prepared standard curve.

For flow cytometry experiments, all cells were plated at a density of 100000 cells per well in six-well plates the night before treatment. Cells were then treated with 25 μM NP-TMZ-CTX or NP-TMZ-NA in 1 mL of fully supplemented DMEM for 4 h. Cells were washed three times with PBS containing 2.5% FBS and detached with 1 mL of a trypsin/EDTA solution. Cells were suspended in 1 mL of PBS containing 2.5% FBS. Analysis of at least 10000 cells for each sample was performed on a BD LSR II flow cytometer (Becton Dickinson). NP fluorescence was detected in the CY5 channel, and data were analyzed using the FlowJo software package (Tree Star Inc., Ashland, OR).

For fluorescence imaging experiments, all cells were plated at a density of 100000 cells per well on poly-L-lysine-coated glass coverslips in 24-well plates the night before treatment. Cells were then treated with 100 μM NP-TMZ or NP-TMZ-CTX in 1 mL of fully supplemented DMEM for 12 h. Cells were washed three times with PBS and fixed in 4% formaldehyde for 30 min. Cell membranes were stained with WGA-AF488 for 15 min. The cells were then mounted on microscope slides using Prolong Gold antifade solution containing DAPI for staining of cell nuclei. NP-TMZ-CTX uptake was analyzed using fluorescence microscopy on a DeltaVision Elite (GE Healthcare, Piscataway, NJ) deconvolution imaging system with an Olympus IX71 inverted microscope with a 60× oil immersion lens. Fluorophores were excited by a solid-state light engine with seven excitation bands at 390, 440, 475, 510, 545, 580, and 640 nm. Emissions from DAPI, WGA-488, and AF647 were detected by a standard filter set (DAPI, FITC, TRITC, and Cy5).

In Vivo BBB Permeability Study. All mice were housed at the University of Washington in a pathogen-free environment under protocols approved by the Institutional Animal Care and Use Committee (IACUC). C57BL6 wild-type mice (Charles River, Wilmington, MA) were injected through the tail vein with 100 μL of 2 mg/mL nanoparticles. Each animal was euthanized 0.5 and 2 h postinjection, and brain tissues were dissected. Tissues were then embedded in OCT and kept frozen at −80 °C until they were needed. The frozen tissues were sliced in 12 μm thick sections and mounted on

DOI: 10.1021/am5092165
ACS Appl. Mater. Interfaces 2015, 7, 6674–6682

Table 1. Physicochemical Properties of Chi-TMZ-Bt, NP-TMZ-NA, and NP-TMZ-CTX

name	TMZ loading (wt %)[a]	loading (%) of TMZ added[a]	hydrodynamic diameter in PBS (nm)[b]	hydrodynamic diameter in DMEM and 2.5% FBS (nm)[b]	ζ potential at pH 7.4 (mV)[c]
Chi-TMZ-Bt	5.4 ± 0.6	24.2 ± 2.1	38 ± 7	40 ± 5	3.9 ± 5.3
NP-TMZ-NA	5.0 ± 0.5	not available	45 ± 8	53 ± 9	−2.9 ± 3.7
NP-TMZ-CTX	4.9 ± 0.5	not available	47 ± 8	57 ± 18	−1.8 ± 4.3

[a]Mean ± standard deviation. [b]Size ± PDI width. [c]ζ potential ± ζ deviation.

glass slides. Slides were then washed with TBS with 0.025% Triton X-100 and blocked in 10% normal serum with 1% BSA in tris(hydroxymethyl)aminomethane-buffered saline (TBS) for 2 h. Slides were then rinsed and stained with rabbit anti-mouse CD31 primary antibody and goat anti-rabbit Fc secondary antibody-FITC conjugate according to instructions provided by Abcam. Coverslips were then mounted on microscope slides using Prolong Gold antifade solution containing DAPI for staining of cell nuclei. Images were acquired on an LSM 780 NLO confocal fluorescence microscope (Carl Zeiss Inc., Peabody, MA) equipped with a 63× oil immersion lens and appropriate filters.

Statistical Analysis. All experiments were conducted in triplicate unless stated otherwise. Acquired data were expressed as the means ± the standard deviation. Statistical significance was determined using a Student's *t* test. *P* values of <0.05 (one asterisk), <0.01 (two asterisks), and <0.001 (three asterisks) were considered significant.

RESULTS

Synthesis of Polymers, Protein Conjugates, and NPs. The structure and synthesis of NP-TMZ-CTX are shown in Scheme 1. NP-TMZ-CTX is comprised of a chitosan core loaded with TMZ and biotin (Chi-TMZ-Bt) and a shell containing CTX targeting ligands attached to AF647-conjugated neutravidin [NA-AF647-CTX (Scheme 1A)]. Chi-TMZ-Bt was synthesized through nucleophilic reactions of amine groups on chitosan-*g*-PEG with biotin-PEG-valeric acid succinimidyl ester and TMZA chloride (Scheme 1B). NA-AF647-CTX was synthesized through linking NA with thiolated CTX using a short, heterobifunctional PEG chain (Scheme 1C). The final product, NP-TMZ-CTX, was synthesized by simply combining Chi-TMZ-Bt and NA-AF647-CTX at a 1:1 molar ratio of Bt to NA (Scheme 1D) and did not require subsequent purification.

NP Properties and Controlled Drug Release. The intermediates Chi-TMZ-Bt and NA-AF647-CTX were characterized by UV−vis to quantify the ratio of their components. The TMZ loading of Chi-TMZ-Bt was 5.4 ± 0.6 wt % (Table 1) as determined by UV−vis absorbance at 328 nm of active TMZ (degradation product MTIC does not absorb at this wavelength). The size and ζ potential of Chi-TMZ-Bt, as characterized by DLS, were 38 ± 7 nm and 3.9 ± 5.3 mV, respectively (Table 1 and Figure 1B,C). There were 1.1 AF647 fluorophore and 2.1 CTX molecules per NA-AF647-CTX molecule, respectively.

NP-TMZ-CTX was characterized by TEM (Figure 1A) as being roughly spherical. The surface of NP was enhanced by uranyl acetate staining as dark fringe. The size of NP under TEM was ∼35 nm. NP-TMZ-CTX and NP-TMZ-NA were also characterized by UV−vis for TMZ loading and DLS for hydrodynamic size and ζ potential. Both NP-TMZ-CTX and NP-TMZ-NA contained similar amounts of TMZ [4.9 ± 0.5 and 5.0 ± 0.5 wt %, respectively (Table 1)]. The difference between TEM size and hydrodynamic size (a few nanometers) is caused by hydration layers associated with NPs. Additionally, the hydrodynamic sizes in PBS and ζ potentials at pH 7.4 of NP-TMZ-CTX and NP-TMZ-NA were similar (Table 1 and Figure 1A,B). Importantly, NP-TMZ-CTX was highly stable in PBS and cell culture media, showing no change in size over 14 days (Figure 1C).

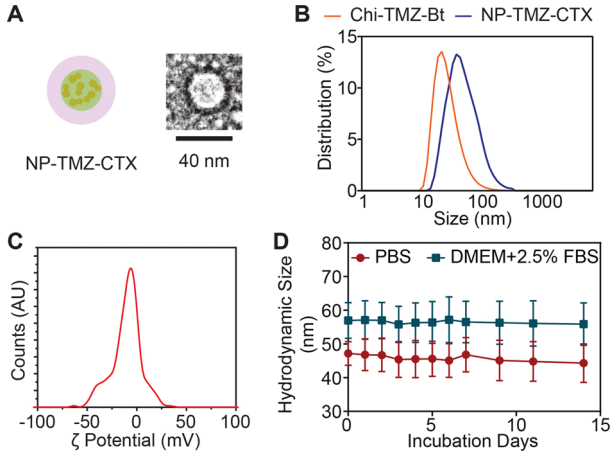

Figure 1. Physicochemical properties. (A) Schematic representation of NP-TMZ-CTX and TEM image of a single NP. (B) Hydrodynamic size distributions for NP-TMZ-Bt (orange) and NP-TMZ-CTX (blue) in PBS. (C) ζ potential distribution of as-synthesized NP-TMZ-CTX. (D) Hydrodynamic size of NP-TMZ-CTX in PBS (orange) and DMEM with 2.5% FBS (blue) over a time period of 14 days. Error bars represent the standard error of the mean.

The aqueous stability of TMZ in NP-TMZ-CTX was tested at pH 7.4, 6.4, 5.5, and 4.5, as well as in serum. The results (Figure 2A) showed that the stability of TMZ, as measured by the half-life of the remaining active TMZ, was significantly increased when it was bound to the NP (Figure 2B). For comparison, the half-life of free TMZ at pH 7.4 is only 1.8 h,[10] while the half-life of NP-TMZ-CTX is 13.4 h. At pH 4.5, TMZ bound to the NP had a marked half-life of 95.8 h. In serum, the half-life of NP-bound TMZ was 21.3 h.

Dose−Response Results. To determine the targeted therapeutic efficacy of NP-TMZ-CTX, human GBM cells were treated with various doses of NP-TMZ-CTZ, NP-TMZ-NA, and free TMZ for 72 h and cell viability was determined using the CellTiter-Glo assay. The dose−response curves for NP-TMZ-CTX, nontargeting control NP-TMZ-NA, and free TMZ are shown in Figure 3A. NP-TMZ-CTX achieved >50% cell killing (IC_{50}) at the lowest TMZ dose, indicating NP-TMZ-CTX was most effective against all three cell lines. The IC_{50} values for NP-TMZ-CTX in U-118 MG, SF767, and GBM6 cells were 86.5, 66.5, and 119.8 μM, respectively. The IC_{50} values of NP-TMZ-NA and free TMZ were in the range of 220−800 μM for all three cell lines. NP-TMZ-CTX achieved an at least 50% reduction in IC_{50} compared to those of NP-TMZ-NA and free TMZ.

Cellular Uptake of NP-TMZ-CTX and NP-TMZ-NA. U-118 MG, SF767, and GBM6 cells were incubated with NP-TMZ-CTX or NP-TMZ-NA as a control at TMZ concentrations of 5, 25, and 250 μM. The targeting ability of NP-

DOI: 10.1021/am5092165
ACS Appl. Mater. Interfaces 2015, 7, 6674−6682

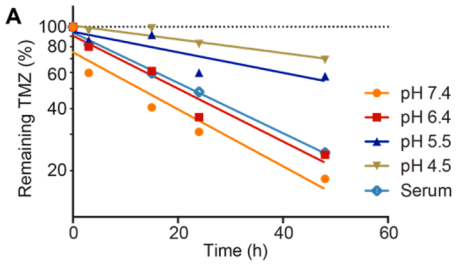

B

Type	Condition	Half-Life (h)
TMZ	PBS, pH 7.4	1.8
NP-TMZ-CTX	PBS, pH 7.4	13.4
NP-TMZ-CTX	PBS, pH 6.4	20.7
NP-TMZ-CTX	PBS, pH 5.5	56.7
NP-TMZ-CTX	PBS, pH 4.5	95.8
NP-TMZ-CTX	Fetal Bovine Serum	21.3

Figure 2. TMZ degradation profile under various conditions. (A) Plot of remaining active TMZ vs time of NP-TMZ-CTX incubated at pH 7.4, 6.4, 5.5, and 4.5 in PBS, as well as in fetal bovine serum. (B) Calculated half-lives of TMZ and NP-TMZ-CTX under various conditions. The half-life of free TMZ was reported previously.[10]

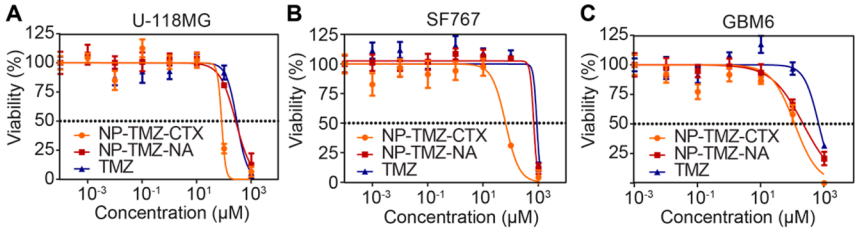

D

	IC_{50} (μM)					
	NP-TMZ-CTX		NP-TMZ		TMZ	
	Mean	SD	Mean	SD	Mean	SD
U118	86.5	0.1	273.9	0.2	302.3	0.6
SF767	66.0	0.1	771.4	0.4	789.1	0.9
GBM6	119.8	1.0	222.0	0.7	686.1	1.0

Figure 3. Therapeutic efficacy of NP-TMZ-CTX, NP-TMZ, and free TMZ as determined by the CellTiter-Glo assay. Dose−response curves in (A) U-118MG, (B) SF767, and (C) GBM6 cell lines. (D) IC_{50} values for NP-TMZ-CTX, NP-TMZ, and free TMZ in the three cell lines.

TMZ-CTX was assessed by fluorescence. An ∼2-fold increase in fluorescence intensity was observed in cells treated with NP-TMZ-CTX as compared to that seen upon NP-TMZ-NA treatment for all three cell types (Figure 4A). The relative fluorescence values [relative fluorescence units (RFU) per microgram of protein] of NP-TMZ-CTX ranged from 120−150 at 5 μM TMZ to 200−230 at 250 μM TMZ, demonstrating a dose-dependent uptake. NP-TMZ-NA showed much lower levels of uptake in these cells, ranging from 30−60 RFU/μg of protein at 5 μM TMZ to 85−120 RFU/μg of protein at 250 μM TMZ.

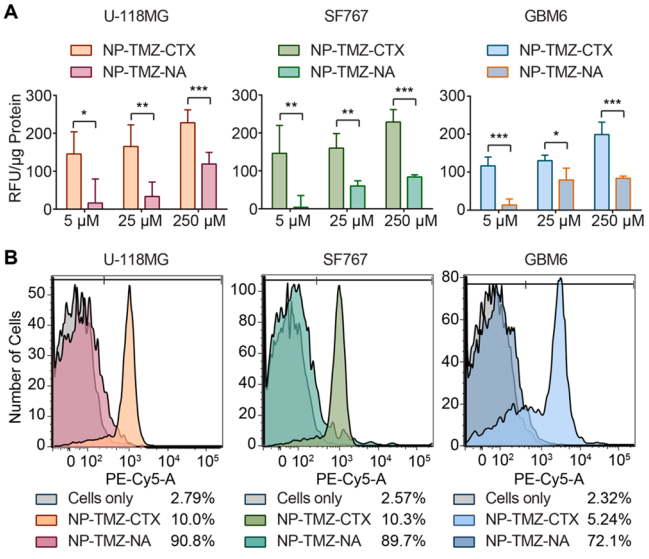

Figure 4. Quantification of cellular uptake of NP-TMZ-CTX and NP-TMZ-NA. (A) Quantification of NP uptake by a microplate reader based on fluorescence intensity. (B) Flow cytometry analysis of U-118 MG, SF767, and GBM6 cells treated with NPs. The percentages of positive cells are provided on the right side of the legend. N.S. indicates not significant. Compared to NP-TMZ-NA as determined by a Student's *t* test, $*P < 0.05$, $**P < 0.01$, and $***P < 0.001$.

The target specificity of NP-TMZ-CTX was further confirmed by flow cytometry. The proportion of cells that contained NP-TMZ-CTX based on Cy5 fluorescence was 90.8, 89.7, and 72.1% for U-118 MG, SF767, and GBM6, respectively (Figure 4B). For cells treated with NP-TMZ-NA, the proportion of positive cells remained below 10.5%.

The distributions of NP-TMZ-CTX and NP-TMZ-NA within the cells were examined by deconvolution fluorescence imaging (Figure 5). NP-TMZ-CTX displayed a strong signal in

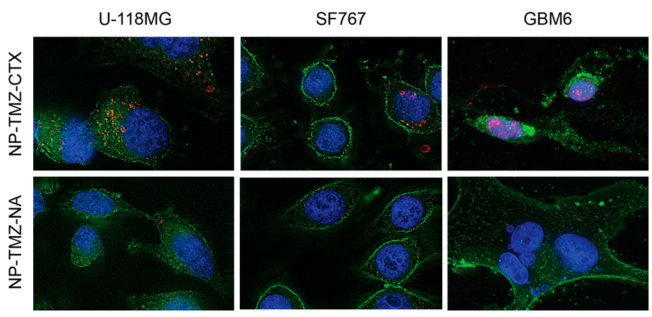

Figure 5. Deconvolved fluorescence images of U-118 MG, SF767, and GBM6 cells treated with NP-TMZ-CTX (top) or NP-TMZ-NA (bottom). Cell nuclei were stained with DAPI (blue); cell membranes were stained with WGA-AF488 (green), and the AF647 signal from NP is colored red.

DOI: 10.1021/am5092165
ACS Appl. Mater. Interfaces 2015, 7, 6674−6682

all three cell lines, whereas little NP-TMZ-NA could be visualized. For U-118 MG and SF767 cells, NPs appeared in the perinuclear region, while for GBM6 cells, the NP signal overlapped with the DAPI signal, indicating their accumulation in the nuclei.

In Vivo BBB Permeability Study. To evaluate BBB permeability of NP-TMZ-CTX, analysis was performed on brain sections of mice 0.5 and 2 h after intravenous injections of NPs (Figure 6). Brain tissue from a mouse receiving no

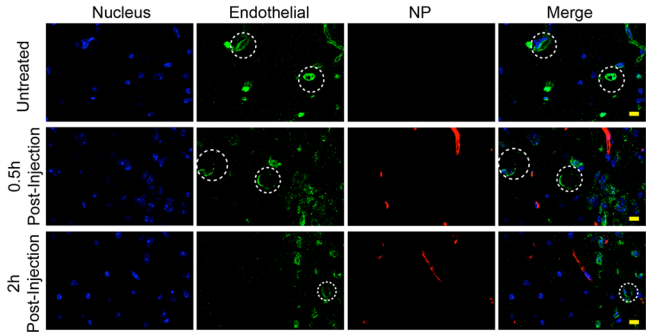

Figure 6. In vivo BBB permeability study. Confocal fluorescence microscopy images of mouse brain tissue sections with one of three treatment conditions: untreated (top), 0.5 h after injection of NP-TMZ-CTX (middle), and 2 h after injection of NP-TMZ-CTX (bottom). Cell nuclei are colored blue; CD31 (endothelial cells) is colored green and NP-TMZ-CTX red. Some blood vessels are highlighted in dashed circles. The scale bar corresponds to 10 μm.

injection showed no signal (red) from NPs (top panel). Images obtained from the mouse 0.5 h after NP administration showed a distribution of NPs throughout the entire image area (not shown) and near blood vessels (middle panel). The extravasation of NPs from blood vessels was more apparent on images obtained from the mouse 2 h after NP administration. There was a significant amount of NPs located in either the region distal from blood vessels or the avascular region of the brain (bottom panel).

DISCUSSION

Synthesis of a target-specific TMZ delivery platform requires rapid and compatible chemical methods for attaching targeting molecules to TMZ delivery vehicles. The most commonly used methods for targeting agent conjugation utilize nucleophilic reaction under neutral or slightly basic conditions, which is detrimental to the stability of TMZ. Therefore, novel chemical methods are needed to synthesize targeted TMZ delivery vehicles to preserve the activity of TMZ. Here we utilized the strong interaction between biotin (Bt) and neutravidin (NA) to attach targeting molecules to our TMZ delivery vehicles. NA is a deglycosylated version of avidin with a higher isoelectric point (pI) with minimal nonspecific interactions.[28] In vivo applications of NA have been reported with no noticeable safety issues.[29,30] Bt-NA binding is the strongest among all noncovalent interactions ($K_d = 10^{-15}$ M) and also possesses fast reaction kinetics. Additionally, the Bt-NA interaction is stoichiometric and stable across a broad pH range[31] as well as under physiological conditions, making it an optimal linker chemistry for targeting attachment of the agent to TMZ-bound NPs.

The synthesis of our NP (NP-TMZ-CTX) is a modular process in which therapeutic cores (Chi-TMZ-Bt) and targeting moieties (NA-AF647-CTX) are synthesized independently. The end product is easily formed in an "on-demand" fashion by mixing the two components at a predetermined ratio to achieve high drug loading. This self-assembly has proven to be effective as many of the targeted nanomedicines in clinical trials utilize the "on-demand" strategy.[32,33] Our NPs do not require subsequent purification, and the end product is monodisperse with a small hydrodynamic size (Figures 1A and 2B). No excessive cross-linking was observed between the four biotin-binding sites on each NA molecule and three biotin sites on each chitosan chain. The size of NP-TMZ-CTX remained around 67.2 nm, even in biological fluid, suggesting it should be able to avoid elimination by the reticuloendothelial system.[34] Furthermore, NP-TMZ-CTX had a near neutral ζ potential that further reduces the level of nonspecific binding to serum proteins, extracellular matrix, and healthy cells.

The fast degradation kinetics of TMZ under physiological conditions would limit its therapeutic potential and hinder its use in standard NP delivery vehicles. Therefore, achieving slower TMZ degradation kinetics is crucial for NP-TMZ-CTX to succeed as a viable drug delivery system. In aqueous solutions, TMZ molecules are converted to 5-(3-methyltriazen-1-yl)imidazole-4-carboxamide (MTIC) and then rapidly to 4-amino-5-imidazole-carboxamide (AIC) that release the methyldiazonium ion responsible for DNA methylation.[10] The conversion of TMZ to MTIC is pH-dependent, with increasing reaction rates at higher pH values. Premature methyldiazonium ion release in the circulatory system could cause off-target DNA damage on hematopoietic stems cells, resulting in neutropenia and other unwanted toxicity, as well as reducing the amount of TMZ available to reach target GBM cells. NP-TMZ-CTX improved the half-life of TMZ at pH 7.4 by almost 7-fold (Figure 2), so it could potentially reduce the level of methyldiazonium ion release in circulation. The improvement of half-life was probably caused by the encapsulation of TMZ within the NP core, preventing water from reaching TMZ. Furthermore, the increased stability of TMZ when bound to the NP at an acidic pH mimicking the tumor microenvironment is highly important to the trafficking of NP into the cell. The 20 h half-life of NP-bound TMZ at pH 6.5 would ensure active TMZ could be delivered to the intracellular site of action of target cells prior to conversion to MTIC.

The targeting ability of NP delivery vehicles is critical to ensure uptake of NPs by tumor cells and distribution throughout the tumor. CTX is a targeting ligand that binds specifically to glioma and other malignant cells.[18] Conjugating CTX to NP surfaces has been shown to help the intratumoral diffusion of these NPs.[35] By combining a greater half-life of TMZ and specific targeting of CTX, we could reduce the overall administrated dose of TMZ. Therefore, it could potentially reduce its bone marrow toxicity and other off-target effects. We examined the uptake of NP-TMZ-CTX compared to that of NP-TMZ-NA in various human GBM cells, including U-118 MG, SF767, and GBM6. U-118 MG is a commonly used GBM cell line that is sensitive to TMZ.[36] SF767 is a commonly used therapy-resistant cell line because of its resistance to radiation and TMZ therapies.[26] GBM6 is a primary GBM culture that shows high resistance to TMZ.[27] CTX targeting drastically increased the rate of accumulation of NPs in GBM cells by 2−6-fold (Figure 4A,B) compared to that with NP-TMZ-NA, resulting in more TMZ available for DNA methylation. Furthermore, fluorescence microscopy revealed strong signals from NP-TMZ-CTX in all three cell lines,

DOI: 10.1021/am5092165
ACS Appl. Mater. Interfaces 2015, 7, 6674−6682

whereas minimal signals from NP-TMZ-NA could be detected. These results indicated that CTX promoted specific targeting and subsequent uptake of NPs into GBM cells.

NP-TMZ-CTX showed at least 50−90% reduction of the IC_{50} when compared with that with NP-TMZ and free TMZ, indicating that the improved uptake observed with NP-TMZ-CTX correlated with a higher rate of cell killing. The improvements of IC_{50} on SF767 and GBM6 cell lines (Figure 3B) are significant because the therapy-resistant subpopulations of GBM cells are difficult to eradicate and are responsible for the recurrence of tumor.[37] It is intriguing that NP-TMZ-CTX was able to reduce the IC_{50} of TMZ-resistant cells as resistance in SF767 and GBM6 is mediated by a high level of expression of O^6-methylguanine-DNA-methyltransferase (MGMT) that removes the cytotoxic methylated DNA. Therefore, the vast majority of research in overcoming TMZ resistance has focused on inhibiting MGMT activity.[38,39] However, our data suggest that NP-mediated delivery of TMZ can also improve the effects of TMZ on these resistant cells, perhaps because of significantly larger doses of active TMZ reaching the intracellular site of action. These large doses of TMZ are thought to deplete intracellular MGMT. Indeed, this was the rationale behind clinical trials studying how dose-dense schedules of TMZ therapy improve patient outcome.[40] Although the trial did not show extended survival with dose escalation, it is likely that sufficient concentrations could not be delivered to the tumor because of toxicity concerns.[41] NP-TMZ-CTX might offer a solution by improving target-specific uptake and minimizing dose-limiting off-target effects.

We confirmed the ability of NP-TMZ-CTX to escape the neural vasculature by performing a BBB permeability study in wild-type mice injected intravenously with NP-TMZ-CTX. Because wild-type mice have an intact BBB, the accumulation of NPs could not be attributed to BBB disruption, as in the case of advanced stage glioblastoma. One-half hour after NP administration, NPs were near blood vessels (Figure 6, middle panel). This indicates NPs started the process of passing through the BBB. Two hours after NP administration, NPs appeared in regions distant from blood vessels (Figure 6, bottom panel). This result suggests that the NP could traverse avascular region of the brain for a relatively long distance. The BBB permeability of the NP might be attributed to the small size of NP-TMZ-CTX (∼50 nm) and multiple BBB permeation molecules attached on NPs, including TMZ[39,42] and CTX via a receptor-mediated mechanism[39] and chitosan via an absorptive-mediated mechanism.[43]

CONCLUSIONS

We have introduced a novel synthetic method for developing a targeted TMZ delivery system that could protect TMZ from fast degradation under physiological conditions and improve the therapeutic efficacy of TMZ against GBM. The NP contains a biotin-functionalized chitosan core that is covalently conjugated with TMZ that were linked to GBM-specific, surface-bound CTX ligands with fast, stable, and stoichiometric biotin−neutravidin interactions. NP-TMZ-CTX showed higher uptake in GBM cells and was more effective in cell killing than nontargeted NPs and free drug. We further demonstrated that NP-TMZ-CTX can cross the BBB and deliver TMZ into the avascular region of the brain. NP-TMZ-CTX offers hope for the delivery of effective doses of TMZ specifically to GBM cells while minimizing dose-limiting toxicity with respect to other healthy tissues. This NP-based delivery system can be broadly applied to various applications as it can be tailored to incorporate various therapeutics that are otherwise unstable or insoluble under physiological conditions. Additionally, the targeting ligand attachment method could be easily modified to other bioorthogonal linkage chemistries such as trans-cyclooctyne-tetrazine reaction pairs.

AUTHOR INFORMATION

Corresponding Author

*Department of Materials Science and Engineering, University of Washington, 302L Roberts Hall, Box 352120, Seattle, WA 98195. E-mail: mzhang@uw.edu. Telephone: (206) 616-9356. Fax: (206) 543-3100.

Notes

The authors declare no competing financial interest.

ACKNOWLEDGMENTS

This work is supported by Grants R01CA161953, R01EB006043, R21EB014572, and R01CA134213 from the National Institutes of Health (NIH) and National Cancer Institute (NCI) and Grant UW-CGF 65-6330 from the University of Washington. C.F. acknowledges support from a National Science Foundation/NCI IGERT Fellowship, and F.M.K., Z.R.S., and Q.M. acknowledge support from an NIH Ruth L. Kirschstein T32 Fellowship (T32CA138312). F.M.K. also acknowledges support from an American Brain Tumor Association Fellowship in Honor of Susan Kramer. K.W. acknowledges support from the University of Washington College of Engineering Dean's Fellowship. We acknowledge lab assistance from Chris Dayringer and Zhixing Wang. We thank the FHCRC Shared Resources Scientific Imaging Core for their assistance with deconvolution microscopy, confocal microscopy, and image analysis. We thank the Sarkaria lab at the Mayo Clinic for providing the GBM6 cells.

REFERENCES

(1) Ostrom, Q. T.; Gittleman, H.; Liao, P.; Rouse, C.; Chen, Y.; Dowling, J.; Wolinsky, Y.; Kruchko, C.; Barnholtz-Sloan, J. Cbtrus Statistical Report: Primary Brain and Central Nervous System Tumors Diagnosed in the United States in 2007−2011. *Neuro-Oncology (Cary, NC, U.S.)* **2014**, *16* (Suppl. 4), iv , 1−63.

(2) Wen, P. Y.; Kesari, S. Malignant Gliomas in Adults. *N. Engl. J. Med.* **2008**, *359*, 492−507.

(3) Huse, J. T.; Holland, E.; DeAngelis, L. M. Glioblastoma: Molecular Analysis and Clinical Implications. *Annu. Rev. Med.* **2013**, *64*, 59−70.

(4) Omuro, A. Glioblastoma and Other Malignant Gliomas. *JAMA, J. Am. Med. Assoc.* **2013**, *310*, 1842.

(5) Parsons, D. W.; Jones, S.; Zhang, X.; Lin, J. C. H.; Leary, R. J.; Angenendt, P.; Mankoo, P.; Carter, H.; Siu, I.-M.; Gallia, G. L.; Olivi, A.; McLendon, R.; Rasheed, B. A.; Keir, S.; Nikolskaya, T.; Nikolsky, Y.; Busam, D. A.; Tekleab, H.; Diaz, L. A.; Hartigan, J.; Smith, D. R.; Strausberg, R. L.; Marie, S. K. N.; Shinjo, S. M. O.; Yan, H.; Riggins, G. J.; Bigner, D. D.; Karchin, R.; Papadopoulos, N.; Parmigiani, G.; Vogelstein, B.; Velculescu, V. E.; Kinzler, K. W. An Integrated Genomic Analysis of Human Glioblastoma Multiforme. *Science* **2008**, *321*, 1807−1812.

(6) Chamberlain, M. C. Bevacizumab for the Treatment of Recurrent Glioblastoma. *Clin. Med. Insights: Oncol.* **2011**, *5*, 117−129.

(7) Gilbert, M. R.; Dignam, J. J.; Armstrong, T. S.; Wefel, J. S.; Blumenthal, D. T.; Vogelbaum, M. A.; Colman, H.; Chakravarti, A.; Pugh, S.; Won, M.; Jeraj, R.; Brown, P. D.; Jaeckle, K. A.; Schiff, D.; Stieber, V. W.; Brachman, D. G.; Werner-Wasik, M.; Tremont-Lukats, I. W.; Sulman, E. P.; Aldape, K. D.; Curran, W. J., Jr.; Mehta, M. P. A

DOI: 10.1021/am5092165
ACS Appl. Mater. Interfaces 2015, 7, 6674−6682

Randomized Trial of Bevacizumab for Newly Diagnosed Glioblastoma. *N. Engl. J. Med.* **2014**, *370*, 699−708.
(8) Zhang, J.; Stevens, M. F.; Bradshaw, T. D. Temozolomide: Mechanisms of Action, Repair and Resistance. *Curr. Mol. Pharmacol.* **2012**, *5*, 102−114.
(9) Quinn, J. A.; Jiang, S. X.; Reardon, D. A.; Desjardins, A.; Vredenburgh, J. J.; Rich, J. N.; Gururangan, S.; Friedman, A. H.; Bigner, D. D.; Sampson, J. H.; McLendon, R. E.; Herndon, J. E., II; Walker, A.; Friedman, H. S. Phase II Trial of Temozolomide Plus O6-Benzylguanine in Adults with Recurrent, Temozolomide-Resistant Malignant Glioma. *J. Clin. Oncol.* **2009**, *27*, 1262−1267.
(10) Patil, R.; Portilla-Arias, J.; Ding, H.; Inoue, S.; Konda, B.; Hu, J.; Wawrowsky, K. A.; Shin, P. K.; Black, K. L.; Holler, E.; Ljubimova, J. Y. Temozolomide Delivery to Tumor Cells by a Multifunctional Nano Vehicle Based on Poly(B-L-Malic Acid). *Pharm. Res.* **2010**, *27*, 2317−2329.
(11) Braun, K.; Wiessler, M.; Ehemann, V.; Pipkorn, R.; Spring, H.; Debus, J.; Didinger, B.; Koch, M.; Muller, G.; Waldeck, W. Treatment of Glioblastoma Multiforme Cells with Temozolomide-Bioshuttle Ligated by the Inverse Diels-Alder Ligation Chemistry. *Drug Des., Dev. Ther.* **2009**, *2*, 289−301.
(12) Veiseh, O.; Sun, C.; Fang, C.; Bhattarai, N.; Gunn, J.; Kievit, F.; Du, K.; Pullar, B.; Lee, D.; Ellenbogen, R. G.; Olson, J.; Zhang, M. Specific Targeting of Brain Tumors with an Optical/Magnetic Resonance Imaging Nanoprobe across the Blood-Brain Barrier. *Cancer Res.* **2009**, *69*, 6200−6207.
(13) Kievit, F. M.; Veiseh, O.; Fang, C.; Bhattarai, N.; Lee, D.; Ellenbogen, R. G.; Zhang, M. Chlorotoxin Labeled Magnetic Nanovectors for Targeted Gene Delivery to Glioma. *ACS Nano* **2010**, *4*, 4587−4594.
(14) Graf, N.; Mokhtari, T. E.; Papayannopoulos, I. A.; Lippard, S. J. Platinum(IV)-Chlorotoxin (Ctx) Conjugates for Targeting Cancer Cells. *J. Inorg. Biochem.* **2012**, *110*, 58−63.
(15) Huang, R.; Ke, W.; Han, L.; Li, J.; Liu, S.; Jiang, C. Targeted Delivery of Chlorotoxin-Modified DNA-Loaded Nanoparticles to Glioma via Intravenous Administration. *Biomaterials* **2011**, *32*, 2399−2406.
(16) Sun, C.; Fang, C.; Stephen, Z.; Veiseh, O.; Hansen, S.; Lee, D.; Ellenbogen, R. G.; Olson, J.; Zhang, M. Tumor-Targeted Drug Delivery and MRI Contrast Enhancement by Chlorotoxin-Conjugated Iron Oxide Nanoparticles. *Nanomedicine* **2008**, *3*, 495−505.
(17) Sun, C.; Veiseh, O.; Gunn, J.; Fang, C.; Hansen, S.; Lee, D.; Sze, R.; Ellenbogen, R. G.; Olson, J.; Zhang, M. In Vivo MRI Detection of Gliomas by Chlorotoxin-Conjugated Superparamagnetic Nanoprobes. *Small* **2008**, *4*, 372−379.
(18) Veiseh, M.; Gabikian, P.; Bahrami, S.-B.; Veiseh, O.; Zhang, M.; Hackman, R. C.; Ravanpay, A. C.; Stroud, M. R.; Kusuma, Y.; Hansen, S. J.; Kwok, D.; Munoz, N. M.; Sze, R. W.; Grady, W. M.; Greenberg, N. M.; Ellenbogen, R. G.; Olson, J. M. Tumor Paint: A Chlorotoxin:Cy5.5 Bioconjugate for Intraoperative Visualization of Cancer Foci. *Cancer Res.* **2007**, *67*, 6882−6888.
(19) Veiseh, O.; Gunn, J. W.; Kievit, F. M.; Sun, C.; Fang, C.; Lee, J. S. H.; Zhang, M. Inhibition of Tumor-Cell Invasion with Chlorotoxin-Bound Superparamagnetic Nanoparticles. *Small* **2008**, *5*, 256−264.
(20) Veiseh, O.; Sun, C.; Gunn, J.; Kohler, N.; Gabikian, P.; Lee, D.; Bhattarai, N.; Ellenbogen, R.; Sze, R.; Hallahan, A.; Olson, J.; Zhang, M. Optical and MRI Multifunctional Nanoprobe for Targeting Gliomas. *Nano Lett.* **2005**, *5*, 1003−1008.
(21) Mortensen, J. H.; Jeppesen, M.; Pilgaard, L.; Agger, R.; Duroux, M.; Zachar, V.; Moos, T. Targeted Antiepidermal Growth Factor Receptor (Cetuximab) Immunoliposomes Enhance Cellular Uptake in Vitro and Exhibit Increased Accumulation in an Intracranial Model of Glioblastoma Multiforme. *J. Drug Delivery* **2013**, *2013*, 209205.
(22) Yoon, D. J.; Kwan, B. H.; Chao, F. C.; Nicolaides, T. P.; Phillips, J. J.; Lam, G. Y.; Mason, A. B.; Weiss, W. A.; Kamei, D. T. Intratumoral Therapy of Glioblastoma Multiforme Using Genetically Engineered Transferrin for Drug Delivery. *Cancer Res.* **2010**, *70*, 4520−4527.
(23) Bhattarai, N.; Matsen, F. A.; Zhang, M. PEG-Grafted Chitosan as an Injectable Thermoreversible Hydrogel. *Macromol. Biosci.* **2005**, *5*, 107−111.
(24) Arrowsmith, J.; Jennings, S. A.; Clark, A. S.; Stevens, M. F. G. Antitumor Imidazotetrazines. 41. Conjugation of the Antitumor Agents Mitozolomide and Temozolomide to Peptides and Lexitropsins Bearing DNA Major and Minor Groove-Binding Structural Motifs. *J. Med. Chem.* **2002**, *45*, 5458−5470.
(25) Deshane, J.; Garner, C. C.; Sontheimer, H. Chlorotoxin Inhibits Glioma Cell Invasion Via Matrix Metalloproteinase-2. *J. Biol. Chem.* **2003**, *278*, 4135−4144.
(26) Bobola, M. S.; Kolstoe, D. D.; Blank, A.; Silber, J. R. Minimally Cytotoxic Doses of Temozolomide Produce Radiosensitization in Human Glioblastoma Cells Regardless of Mgmt Expression. *Mol. Cancer Ther.* **2010**, *9*, 1208−1218.
(27) Carlson, B. L.; Grogan, P. T.; Mladek, A. C.; Schroeder, M. A.; Kitange, G. J.; Decker, P. A.; Giannini, C.; Wu, W.; Ballman, K. A.; James, C. D.; Sarkaria, J. N. Radiosensitizing Effects of Temozolomide Observed in Vivo Only in a Subset of O6-Methylguanine-DNA Methyltransferase Methylated Glioblastoma Multiforme Xenografts. *Int. J. Radiat. Oncol., Biol., Phys.* **2009**, *75*, 212−219.
(28) Marttila, A. T.; Laitinen, O. H.; Airenne, K. J.; Kulik, T.; Bayer, E. A.; Wilchek, M.; Kulomaa, M. S. Recombinant Neutralite Avidin: A Non-Glycosylated, Acidic Mutant of Chicken Avidin That Exhibits High Affinity for Biotin and Low Non-Specific Binding Properties. *FEBS Lett.* **2000**, *467*, 31−36.
(29) Tseng, C. L.; Wu, S. Y.; Wang, W. H.; Peng, C. L.; Lin, F. H.; Lin, C. C.; Young, T. H.; Shieh, M. J. Targeting Efficiency and Biodistribution of Biotinylated-Egf-Conjugated Gelatin Nanoparticles Administered via Aerosol Delivery in Nude Mice with Lung Cancer. *Biomaterials* **2008**, *29*, 3014−3022.
(30) Hama, Y.; Urano, Y.; Koyama, Y.; Choyke, P. L.; Kobayashi, H. Activatable Fluorescent Molecular Imaging of Peritoneal Metastases Following Pretargeting with a Biotinylated Monoclonal Antibody. *Cancer Res.* **2007**, *67*, 3809−3817.
(31) Nordlund, H. R.; Hytonen, V. P.; Laitinen, O. H.; Uotila, S. T.; Niskanen, E. A.; Savolainen, J.; Porkka, E.; Kulomaa, M. S. Introduction of Histidine Residues into Avidin Subunit Interfaces Allows pH-Dependent Regulation of Quaternary Structure and Biotin Binding. *FEBS Lett.* **2003**, *555*, 449−454.
(32) Davis, M. E.; Zuckerman, J. E.; Choi, C. H. J.; Seligson, D.; Tolcher, A.; Alabi, C. A.; Yen, Y.; Heidel, J. D.; Ribas, A. Evidence of RNAi in Humans from Systemically Administered Sirna via Targeted Nanoparticles. *Nature* **2010**, *464*, 1067−1070.
(33) Farokhzad, O. C.; Jon, S.; Khademhosseini, A.; Tran, T. N.; Lavan, D. A.; Langer, R. Nanoparticle-Aptamer Bioconjugates: A New Approach for Targeting Prostate Cancer Cells. *Cancer Res.* **2004**, *64*, 7668−7672.
(34) Petros, R. A.; Desimone, J. M. Strategies in the Design of Nanoparticles for Therapeutic Applications. *Nat. Rev. Drug Discovery* **2010**, *9*, 615−627.
(35) Fang, C.; Veiseh, O.; Kievit, F.; Bhattarai, N.; Wang, F.; Stephen, Z.; Li, C.; Lee, D.; Ellenbogen, R. G.; Zhang, M. Functionalization of Iron Oxide Magnetic Nanoparticles with Targeting Ligands: Their Physicochemical Properties and in Vivo Behavior. *Nanomedicine* **2010**, *5*, 1357−1369.
(36) Ponten, J.; Macintyre, E. H. Long Term Culture of Normal and Neoplastic Human Glia. *Acta Pathol. Microbiol. Scand.* **1968**, *74*, 465−486.
(37) Pattabiraman, D. R.; Weinberg, R. A. Tackling the Cancer Stem Cells : What Challenges Do They Pose? *Nat. Rev. Drug Discovery* **2014**, *13*, 497−512.
(38) Hegi, M. E.; Liu, L.; Herman, J. G.; Stupp, R.; Wick, W.; Weller, M.; Mehta, M. P.; Gilbert, M. R. Correlation of O6-Methylguanine Methyltransferase (MGMT) Promoter Methylation with Clinical Outcomes in Glioblastoma and Clinical Strategies to Modulate MGMT Activity. *J. Clin. Oncol.* **2008**, *26*, 4189−4199.
(39) Stephen, Z. R.; Kievit, F. M.; Veiseh, O.; Chiarelli, P. A.; Fang, C.; Wang, K.; Hatzinger, S. J.; Ellenbogen, R. G.; Silber, J. R.; Zhang,

DOI: 10.1021/am5092165
ACS Appl. Mater. Interfaces 2015, 7, 6674−6682

M. Redox-Responsive Magnetic Nanoparticle for Targeted Convection-Enhanced Delivery of O6-Benzylguanine to Brain Tumors. *ACS Nano* **2014**, *8*, 10383−10395.
(40) Gilbert, M. R.; Wang, M.; Aldape, K. D.; Stupp, R.; Hegi, M. E.; Jaeckle, K. A.; Armstrong, T. S.; Wefel, J. S.; Won, M.; Blumenthal, D. T.; Mahajan, A.; Schultz, C. J.; Erridge, S.; Baumert, B.; Hopkins, K. I.; Tzuk-Shina, T.; Brown, P. D.; Chakravarti, A.; Curran, W. J., Jr.; Mehta, M. P. Dose-Dense Temozolomide for Newly Diagnosed Glioblastoma: A Randomized Phase III Clinical Trial. *J. Clin. Oncol.* **2013**, *31*, 4085−4091.
(41) Spence, A. M.; Kiem, H. P.; Partap, S.; Schuetze, S.; Silber, J. R.; Peterson, R. A. Complications of a Temozolomide Overdose: A Case Report. *J. Neurooncol.* **2006**, *80*, 57−61.
(42) Mrugala, M. M.; Chamberlain, M. C. Mechanisms of Disease: Temozolomide and Glioblastoma—Look to the Future. *Nat. Clin. Pract. Oncol.* **2008**, *5*, 476−486.
(43) Agyare, E. K.; Curran, G. L.; Ramakrishnan, M.; Yu, C. C.; Poduslo, J. F.; Kandimalla, K. K. Development of a Smart Nano-Vehicle to Target Cerebrovascular Amyloid Deposits and Brain Parenchymal Plaques Observed in Alzheimer's Disease and Cerebral Amyloid Angiopathy. *Pharm. Res.* **2008**, *25*, 2674−2684.

DOI: 10.1021/am5092165
ACS Appl. Mater. Interfaces 2015, 7, 6674−6682